**A progress report for the Latvian Council of Science project conducted within the Fundamental and applied research projects framework "*Engineered surface platform for immobilization of microorganisms*" (lzp-2018/1-0460) on the work done during the 01.12.2018. – 01.03.2019. time frame**

The report includes progress information on the following tasks:

- Quality control of received immobilization platforms
- Surface characterization of the immobilization platforms and satellite samples using photoelectron emission spectroscopy (PES), Fourier transform infrared spectroscopy (FTIR), semi-contact atomic force microscopy (AFM) in topographic and Kelvin probe force microscopy (KPFM) modes
- Development of a cell immobilization technique

## Achieved results

### Quality control of received immobilization platforms

After receiving the immobilization platforms from the manufacturer, they were imaged using scanning electron microscopy (SEM) in secondary electron mode to see whether the shape, size and spacing in between the structures conform to the values stated in the developed model. The measurements acquired from SEM images are given in Table 1. A representative image of the structures is given in Figure 1.

**Table 1.** Comparison of microstructure geometry parameters between the CAD model values and the measured values

| Sample type | Height (modeled), mkm | Height (measured), mkm | Side length (modeled), mkm | Side length (measured), mkm | Gap length (modeled), mkm | Gap length (measured), mkm |
|---|---|---|---|---|---|---|
| 39-1-1 | 3.00 | 4.18 ± 0.12 | 12.00 | 10.72 ± 0.1 | 2.00 | 4.23 ± 0.08 |
| 39-1-2 | 3.00 | - | 3.00 | - | 12.00 | - |
| 39-1-3 | 3.00 | 3.93 ± 0.12 | 12.00 | 10.97 ± 0.1 | 12.00 | 14.77 ± 0.13 |
| 39-1-6 | 12.00 | 5.37 ± 0.14 | 12.00 | 10.4 ± 0.08 | 12.00 | 13.48 ± 0.12 |
| 39-1-7 | 12.00 | 8.56 ± 0.33 | 48.00 | 46.01 ± 2.13 | 2.00 | 4.81 ± 0.32 |
| 39-1-9 | 12.00 | 6.93 ± 0.11 | 48.00 | 45.46 ± 0.12 | 12.00 | 12.78 ± 0.16 |
| 39-1-10 | 12.00 | 6.19 ± 0.05 | 12.00 | 9.44 ± 0.08 | 2.00 | 4.49 ± 0.05 |

The dimensions of the structures are uniform; however, the difference in gap width is two-fold or more for some samples when compared with the technical drawings. This should not cause too many complications during the experiments since the dimensions are comparable to the diameter of certain larger strains of S. cerevisiae yeast cells. The difference in height, however, could cause some complications down the line since the difference between the shortest (3.93 mkm for 39-1-3) and the tallest (8.56 mkm for 39-1-7) structure is about 4.5 mkm which is only a two-fold difference instead of the projected four-fold difference.

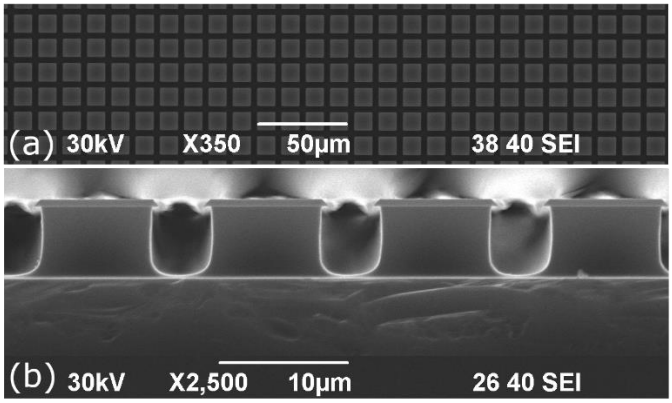


***Figure 1.*** *Representative images of structures present on the surfaces of immobilization platforms (39-1-10, in this case) taken from the top and from the side.*

The modeled structures shape was that of a parallelepiped. The shape of the microstructures on the received immobilization platforms is more akin to a mushroom – with a filleted base and an approx. 0.6 mkm thick cap. However, when viewed from the normal direction the structures are square shaped, and therefore can be accepted as an array of parallelepiped-like structures. Interestingly, the shape of the microstructures located on the surface of immobilization platforms of type 39-1-2 is very similar to a four-sided pyramid proving that the manufacturer can produce the initially discussed shapes, even if by accident. An SEM image of these structures is given in Figure 2. Since the structures on platforms of type 39-1-2 have a shape that differs from the requested parallelepiped-like shape their dimensions can't be compared with those of the microstructures located on the other platforms.

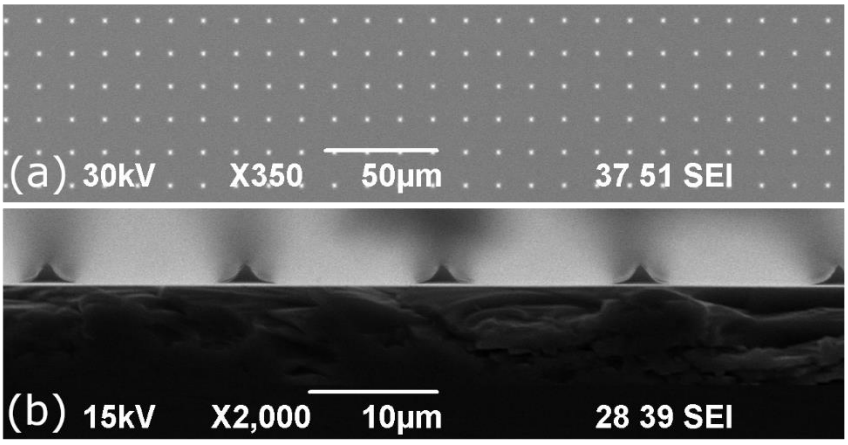


***Figure 2.*** *SEM images of microstructures present on the surface of 39-1-2 type immobilization platforms taken from the top and from the side.*

To check the local relative chemical composition of the surfaces of the immobilization platforms SEM investigations in back-scattered electron imaging in compositional mode were performed. A representative image taken from the top of a 39-1-10-type immobilization platform was is given in Figure 3.

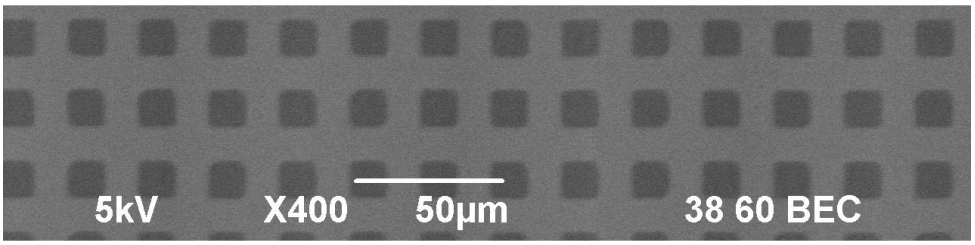


***Figure 3.*** *SEM image in back-scattered electron detection mode taken from the top of an immobilization platform (39-1-10).*

The images show a pattern of darker patches on a lighter background. In back-scattered electron detection mode (compositional) low-brightness images represent regions primarily composed of lower atomic weight elements while high-brightness images represent regions primarily composed of higher atomic weight elements. While the method can't determine the type of element present on the surface it can show relative changes in composition between different locations on a samples surface. In the case of Figure 3 the tops of the microstructures are darker than the surrounding areas which can be explained by a presence of a relatively thick silicon dioxide layer on the tops of the structures and the surrounding areas being composed primarily from silicon. This indeed was the case because during the manufacturing of the structures a layer of $SiO_2$ was deposited onto the surface of a Si wafer to create a protection layer that would help shape the structures during etching. Thus, it can be concluded that the top 0.6 mkm layer of the structures is composed of $SiO_2$ and the area surrounding the structures as well as the sides of the structures are composed of Si with a thin layer of natural $SiO_2$ on its surface.

## Surface characterization of the immobilization platforms and satellite samples

With the surface geometry and relative composition of the immobilization platforms checked the next step was to characterize the samples nanoscale roughness and local and global surface potential values as well as their chemical composition.

Nano-scale roughness measurements of the surfaces of microstructured samples was measured for six sample groups. The surface of the samples was divided into two sets of regions of interest – the top parts of the structures (referred to as "plateaus") and the base on which the samples are positioned (referred to as "valleys"). Since previous tests showed that the composition of these two types of surfaces is different, therefore, it was necessary to perform nano-scale roughness measurements separately on both plateaus and valleys.

From each of the studied sample groups four samples were selected at random meaning the measurements were performed on 24 samples in total. For each sample at least 10 measurements were performed on the surfaces of randomly chosen plateaus. Due to geometrical constraints caused by the height of the samples (~ 4 mkm) and the shape of the probe (distances between the columns for some samples were close to 4 mkm, while the probes cross-sectional diameter at 4 mkm distance from the surface is approximately equal to the distance between the columns, fully constraining the probes movement) as well as the maximum displacement of the scanning piezo tube of the AFM (no more than 3 mkm), the scanning of the valleys themselves was impossible. However, SEM studies of the samples

surface showed that the relative composition of the base layer is the same at all points. Therefore, instead of measuring the nano-scale roughness in the inaccessible valleys, it was decided to perform nano-scale roughness measurements in equivalent areas close to the samples edge since those regions provided enough space for the probe to be able to move. Thus, for each sample at least 10 measurements were performed in regions equivalent to the valleys in between the structures located close to the edge of the sample. A total of at least 240 regions were scanned, each being 7x7 mkm2 in area. The square of the scan areas was selected based on the single largest scannable area of a plateau for a sample type with the smallest plateau surface area, that being sample types 39-1-6 and 39-1-10. The scans were performed using an NT-MDT Solver P47-PRO atomic force microscope (Russia) equipped with TipsNano NSG01/Pt metal coated scanning probes in semi-contact (tapping) mode. The lateral resolution of each scan was at least 14 nm/pixel while height resolution was on the order of 0.1 nm.

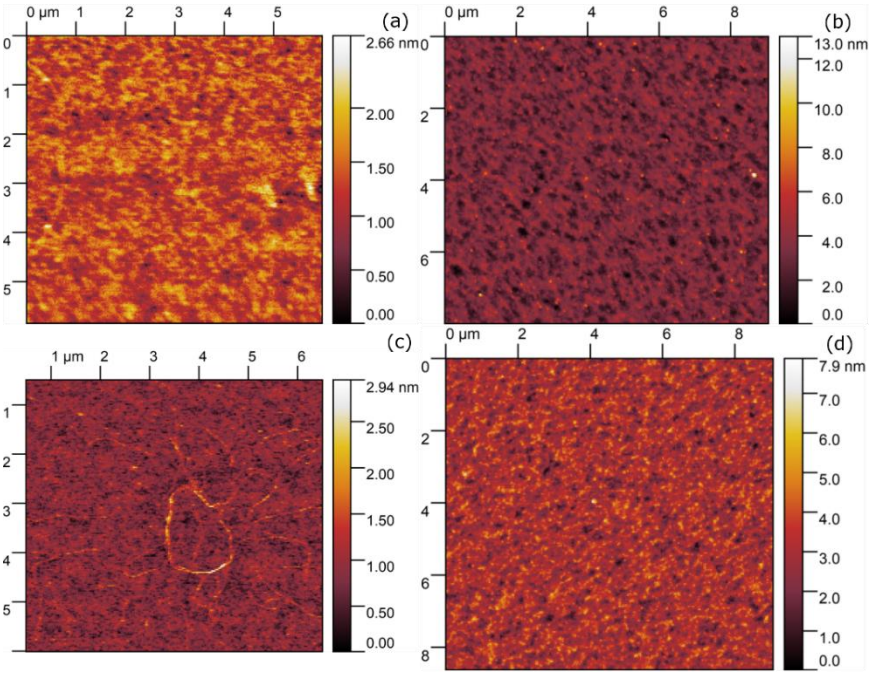


***Figure 4.*** *Representative sample surface nanoscale topography scans taken using semi-contact AFM: (a), (c) surface of a structures plateau (39-1-6 and 39-1-10, respectively); (b), (d) surface of a valley (39-1-6 and 39-1-10, respectively).*

The average surface roughness for plateaus and based on 120 scans was 1.1±0.3 nm. For valleys this value was higher averaging at 4±1.3 nm also based on 120 scans. The average roughness values were a) distinct for each specific surface type (valleys vs. plateaus) and b) similar among representatives of the same surface type. Therefore, it was concluded that these values are sufficiently low not to cause any sizeable interference while conducting cell deposition tests.

In parallel with nano-scale topography measurements surface potential measurements were performed using Kelvin probe force microscopy in amplitude modulation mode (AM-KPFM) to identify the electrical potential of the surfaces of the samples. Since AM-KPFM provides readings both for topography and surface potential these data were acquired in tandem. Therefore, the AFM microscope, the probes used for the measurement of surface potential, the total number of scans and the scan size were the same as the ones used for topography measurements. The lateral resolution for AM-KPFM, however, differs since for surface potential it also relies, among other factors, on the hover distance between the probe and the sample. Therefore, the lateral resolution for surface potential was 35 nm. Voltage resolution

was about 2 mV. As a reference each time before and after scanning every sample a scan in AM-KPFM mode of a freshly cleaved surface of a highly oriented pyrolithic graphene (HOPG) test sample was performed and later used to get the actual surface potential of the actual sample. To ensure the electrical contact between the sample and the grounding electrode samples were affixed to a sapphire platform with Amepox Electron 40 AC single component, electrically conductive, silver filled lacquer.

The surface potential values mirrored the topography measurements in that the surface potential of the plateaus differed from that of the valleys. The average surface potential value for valleys of all scanned samples was measured to be 4.49±0.06 V and the average surface potential for plateaus of all scanned samples was measured to be 4.67±0.11 V. Representative images of nanoscale roughness scans as well as the accompanying images acquired through KPFM are given in Figure 4.

Photoelectron emission spectroscopy (PES) was used to characterize the electrical properties of platforms. Because the intensity of the electron emission current is dependent on the incident photon energy such as the emission current being zero until the energy of the incident photon is high enough to cause an electron to jump from an energy state within the material out into the vacuum level the electron work function of a material (the minimal energy needed to allow for an electron to escape from the emitter into the vacuum) was identified. The value of work function is directly connected to the density of the surface charge of the semiconductor of dielectric materials.

PE spectra were taken using a custom-made spectrometer from $SiO_2$ satellite samples and from six out of seven groups of microstructured samples before electrical charge deposition by means of exposure to UV radiation. After placing the samples into the vacuum chamber of the photoelectron emission spectrometer and reducing the pressure inside of the chamber to ~$10^{-5}$ Pa photoelectron emission spectra were acquired in the spectral range of 300 to 200 nm with a rate of 1 nm/s. Measurements were performed on four randomly selected samples from each group in three spots on their surface and then averaged. A total of 28 samples were used, giving a grand total of 84 measurements. The work function value for each sample was calculated using the near-threshold approach (work function is equal to the photon energy, when the PE current is zero). The average acquired value for the work function from the satellite samples was 4.84±0.05 eV and the average acquired value for the work function from all micropatterned samples was 4.47±0.06 eV.

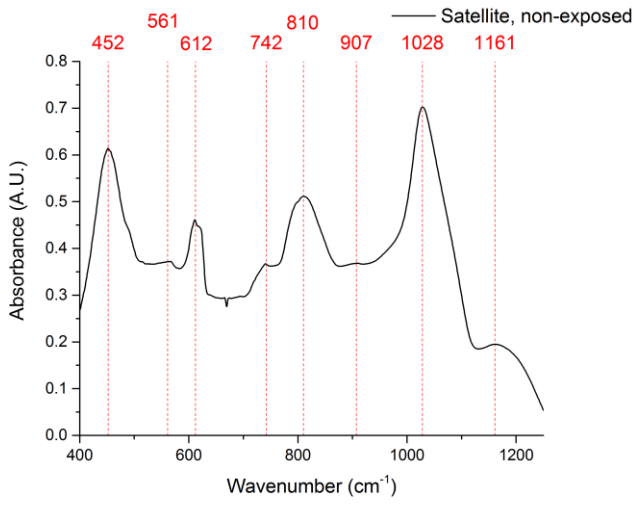


***Figure 5**. ATR FTIR absorption spectrum acquired from satellite samples.*

Attenuated total reflectance (ATR) FTIR (Bruker TENSOR 2, UK) was used throughout the study to see whether exposure to UV radiation might in any way affect the chemical bonds of the samples. However, since these measurements require the sample to be in close contact with the ATR crystal spectra acquisition from micropatterned samples might result in damage to the microscale features. Therefore, it was decided to use flat satellite samples (Si wafers with a 0.6 mkm thick layer of thermally grown SiO2 on top) provided by the manufacturer of the platforms.

Infrared absorption spectra were taken before UV exposure from four randomly selected satellite samples then used to calculate an average spectrum which can be seen in Figure 5. The standard deviation of the averaged spectra peaks' position did not exceed the uncertainty of the wavelength measurement $\pm$2nm guaranteed by the manufacturer of the spectrometer. Spectral analysis in the 400-1200 cm-1 range shows the presence of four very distinct peaks four less distinct peaks. 452 cm-1, 811 cm-1, 1028 cm-1 and 1162 cm-1 corresponding with the bending, symmetric stretching, in-phase asymmetric stretching and out-of-phase asymmetric stretching of Si-O-Si bonds and can be fitted onto the IR spectrum for α-cristobalite, a polymorph of silica that is formed at high temperatures. The less pronounced peaks could correspond to the bending and stretching vibrations of Si-O, Si-O-H and Si-O-D bonds.

## Development of a cell immobilization technique

To seed the cells a yeast immobilization method was developed which consists of 4 steps:

1. Incubation of yeast cells with microstructures on a rotary shaker during 1 h at 30 °C,
2. The short resting period to allow yeast to sediment on the surface of carrier during 20 min (without stirring the suspension),
3. Incubation of samples in distilled water to remove unattached cells,
4. Dehydration of preparations at 30 °C.

Immobilization of the yeasts was performed with suspension of native *Saccharomyces cerevisiae* (Strain 77) yeast taken from the stationary phase of growth after 44 hours of incubation. The suspension was prepared by dissolving 3 g of pressed yeast biomass in 100 ml of water with subsequent dilutions using different ratios (1:50, 1:100 and 1:200). Optical density control was performed for all dilutions. For a dilution of 1:200 the optical absorbance was 0.120 A.U. at 600 nm.

Figure 6 shows the experimental results obtained by performing cell seeding experiments using suspensions with different concentrations of yeast cells.

The most efficient immobilization of cells that would give us the possibility of further microscopical analysis of cell physiological state was reached when a dilution of the yeast suspension was 1:200 ($OD_{600}$ 0.120). Such yeast suspension concentration was used in further experiments.

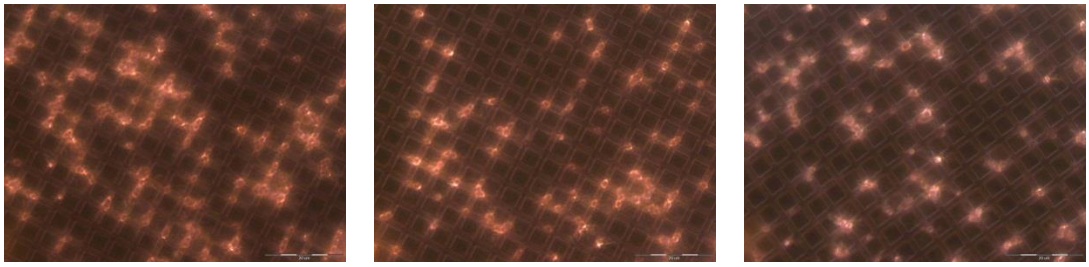

**(a)** **(b)** **(c)**

***Figure 6.*** *Phase-contrast microscopy images that show the results of use of different concentrations of yeast cells used for cell immobilization on microstructures of type 39-1-1. Dilutions of yeast suspension: (a) 50x, (b) 100x, (c) 200x. Objective used 40x, scale bar 20 µm.*

Figure 7 shows the results obtained during experiments to determine the effect of the speed of suspension mixing on yeast cell immobilization. Three rotation speeds were chosen – 50, 80 and 100 rpm. It can be seen in Figure 7C that the best results were obtained with the rotation speed 50 rpm that was used for further experiments.

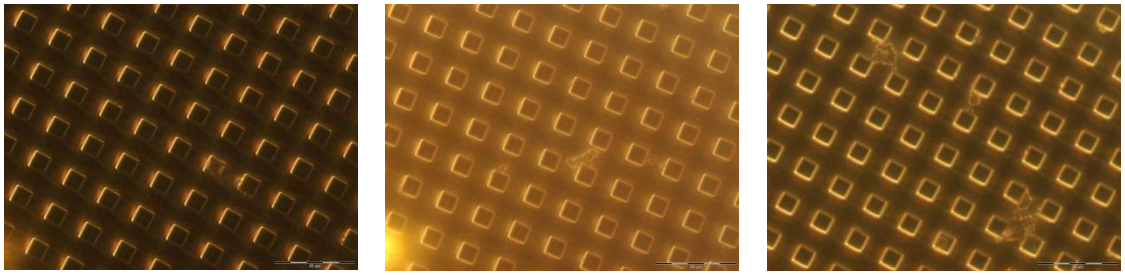

**(a)** **(b)** **(c)**

***Figure 7.*** *Phase-contrast microscopy images of immobilized yeast cells when different rotation speed of microbial suspension was used. Microstructure type 39-1-3. Rotation speed: (a) 100 rpm, (b) 80 rpm, (c) 50 rpm. Objective 40x, scale bar 20 µm.*

Based on these findings the following cell deposition technique was developed:

1. Approximately 0.5 g of baker's yeast (*S. cerevisiae*) should be added to 150 ml of distilled water in a glass beaker then mixed on a magnetic stirrer for 2 minutes or until the suspension becomes uniformly visually opaque.
2. A 1 ml sample of the suspension should be taken to measure its optical density at 600 nm with an UV-VIS spectrometer (in the case of this study – a Thermo Helios Gamma).
    a. If the density is within the required 0,1 – 0,2 AU, then the concentration of cells should be small enough for the deposition experiments.

b. If not part of the suspension should be disposed of and extra distilled water added until it reached a satisfactory AU value. In the case of this study the concentration of baker's yeast in the suspension corresponded to an absorbance value of 0.187 AU and maintained at that value for all deposition experiments.

3. The samples should be placed into a Petri dish and fixed in place at a location that is at a distance of at least half the radius of the dish to exclude the possibility of cells being deposited from a stagnant flow region. The Petri should then be placed on an orbital shaker and filled up with suspension. For the 90 mm Petri dishes used during this study 50 ml of suspension per Petri was added.
4. The Petri should be rotated at 50 RPM for 60 minutes after which the samples are to be kept stationary and in the suspension for 20 minutes.
5. Then the liquid should be slowly and carefully drained with a syringe and the samples should be left to dry for 5 minutes.
6. After that 50 ml of distilled water should be added into the Petri's which then should be once again rotated at 50 RPM for 5 minutes.
7. Lastly the water should be removed with a syringe and the samples should be left to dry in a thermostat for 15 minutes at 30 $^{o}$C.

Steps 5 and 6 are necessary to wash away the cells that did not attach to the surface of the samples.

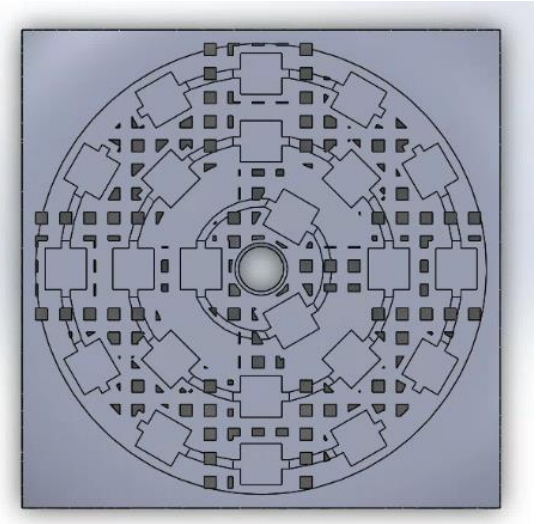

***Figure 8.*** *Sample holder used during cell deposition experiments.*

To keep the samples in place and equidistant from the center of the Petri dish during cell deposition a dedicated sample holder was designed using SOLIDWORKS 2018 and manufactured out of an acrylic photopolymer using stereolithography (Anycubic PHOTON DLP 3D printer, China). The sample holder had sockets for samples that can be located at three different distances from the center of the holder further referred to as "rings". The inner ring (closer to the center) had 3 sockets, the middle ring had 8 sockets and the outer ring had 12 sockets. An image of the holder 3D model is given in Figure 8. During

this study only the outer ring sockets were used as to prevent the deposition of cells that concentrate closer to the center of the vortex. The holder was designed to fit snuggly into a Petri dish with an internal diameter of 90 mm. The side lengths of the square sockets (about 5.05 mm) were adjusted multiple times so that the samples became immobile once inserted into a socket. During its preliminary testing the performance of the holder proved satisfactory at keeping the samples stationary during cell deposition experiments, thus it will be used during every cell deposition procedure.

## Conclusion

The platforms with the micropatterned surfaces were designed and manufactured. The platforms are suitable for further immobilization of yeast cells.

Nanoscale roughness measurements were performed on the plateaus and valleys for multiple samples of different types using semi-contact AFM. Nanoscale roughness values are below 10 nm. Microscale roughness, i.e. the size, shape and spacing between microscale features, was measured using SEM in SE mode and the results were given in a previous section.

Overall surface potential measurements were performed using PES; the results show a difference in work function value between satellite samples and micropatterned samples which can be explained by differences in oxide layer thickness on top of valleys and plateaus. Very little variation was noticed in the work functions of samples micropatterned in different ways. Local surface potential was measured on the plateaus and valleys for multiple samples of different types using AM-KPFM. The surface potential values for the plateaus differ from those measured in valleys, supporting the notion that valleys and plateaus differ in composition.

The layer on top of the microstructures has been identified as a type of thermally grown $SiO_2$ using FTIR spectroscopy performed on satellite samples.

A cell seeding technique to be used during this project has been developed.